

Synthesis and Performance of an Acrylamide Copolymer Containing Nano-SiO₂ as Enhanced Oil Recovery Chemical

Zhongbin Ye,^{1,2} Xiaoping Qin,¹ Nanjun Lai,^{1,2} Qin Peng,^{1,2} Xi Li,^{1,2} Cuixia Li³

¹ State Key Laboratory of Oil and Gas Reservoir Geology and Exploitation, Southwest Petroleum University, Chengdu 610500, People's Republic of China

² College of Chemistry and Chemical Engineering, Southwest Petroleum University, Chengdu 610500, People's Republic of China

³ Department of Petroleum Chemical Engineering, Karamay Vocational & Technical College, Karamay 833600, People's Republic of China

Abstract

A novel copolymer containing nano-SiO₂ was synthesized by free radical polymerization using acrylamide (AM), acrylic acid (AA) and nano-SiO₂ functional monomer (NSFM) as raw materials under mild conditions. The AM/AA/NSFM copolymer was characterized by infrared (IR) spectroscopy, ¹H NMR spectroscopy, elemental analysis, and scanning electron microscope (SEM). It was found that the AM/AA/NSFM copolymer exhibited higher viscosity than the AM/AA copolymer at 500 s⁻¹ shear rate (18.6 mPa·s vs. 8.7 mPa·s). It was also found that AM/AA/NSFM could achieve up to 43.7% viscosity retention rate at 95 °C. Mobility control results indicated that AM/AA/NSFM could establish much higher resistance factor (RF) and residual resistance factor (RRF) than AM/AA under the same conditions (RF: 16.52 vs. 12.17, RRF: 3.63 vs. 2.59). At last, the enhanced oil recovery (EOR) of AM/AA/NSFM was up to 20.10% by core flooding experiments at 65 °C.

1. Introduction

Polymer flooding plays an important role in the field of enhanced oil recovery (EOR) [1, 2]. However, the current widely used polymer, polyacrylamide (PAM) and partially hydrolyzed polyacrylamide (HPAM), cannot completely meet the requirements due to the hydrolysis, degradation and others under high temperature or high salinity [3-6]. Furthermore, PAM and HPAM have poor shear resistance [2-7]. Polymer

molecular chains will be cut off when polymer solution passes through the pump, pipeline, perforation, and porous medium at high speed, so the viscosity of polymer solution will be greatly reduced [1, 7, 8].

Recently, many studies have demonstrated that performance of composite material could be significantly improved by combination or copolymerization with a functional monomer containing nano-SiO₂. The composite material containing Nano-SiO₂, such as polyethylene terephthalate [9], styrene butadiene rubber [10], polyaniline [11], polyimide [12], and nylon 6 [13], may exhibit more satisfactory thermal stability, toughness and strength owing to the effect of physical adsorption, hydrogen bond, Si-O bond, and C-Si bond [10, 12, 14-16]. However, there are no papers about the application of nano-SiO₂ in polymer for flooding to develop temperature tolerance, salt tolerance, and shear resistance of copolymer.

Keeping in mind of these fundamental conditions, herein, a novel nano-SiO₂ functional monomer (NSFM, see Scheme 1) was introduced into AM/AA copolymer aiming to obtain satisfying temperature tolerance, salt tolerance and shear resistance [17-20].

2. Experimental

2.1. Chemicals and Reagents

Ethanol (C₂H₅OH, 99.7%), ammonia (NH₄OH, 28.0%), vinyltriethoxysilane (VTES, 98.0%), acrylic acid (AA, 99.5%), acrylamide (AM, 99.0%), sodium hydrogen sulfite (NaHSO₃, 58.5%), ammonium persulfate ((NH₄)₂S₂O₈, 98.0%), sodium hydroxide (NaOH, 96.0%), sodium chloride (NaCl, 99.5%), magnesium chloride hexahydrate (MgCl₂·6H₂O, 98.0%), calcium chloride anhydrous (CaCl₂, 96.0%), potassium chloride (KCl, 99.5%), sodium sulfate (Na₂SO₄, 99.0%), and sodium bicarbonate (NaHCO₃, 99.5%) were purchased from Chengdu Kelong Chemical Reagent Factory (Sichuan, China). Nano-SiO₂ (10-20 nm) was obtained from Aladdin chemistry (Shanghai, China) Co., Ltd.. All chemicals and reagents were used as received without any further purification. Water was deionized by passing through an

ion-exchange column and doubly distilled.

2.2. Preparation of Nano-SiO₂ Functional Monomer

Firstly, 83.6 mL ethanol, 1.5 g nano-SiO₂, 13.6 mL distilled water and 1.3 mL ammonia were added into a 250 mL round-bottom flask, and the mixture was dispersed with supersonic wave for 30 min. And then, 2.0 mL VTES was added into the stirred solution in the round-bottom flask, and the reaction time was 18 h at 30 °C. After reaction, the product was NSF_M which was separated by centrifugation and washed with distilled water [21-23].

2.3. Synthesis of AM/AA/NSFM

0.05 g NSF_M, 6.50 g AM, 3.45 g AA and a certain amount of distilled water were added into a 100 mL three-necked flask, respectively, and the pH value of the mixture was regulated to 7.0 using sodium hydroxide solution, then the solution with 20% total monomer mass concentration was prepared. 0.05 g NaHSO₃-(NH₄)₂S₂O₈ initiator (mol ratio = 1:1) was taken along with distilled water in the three-necked flask assembled with a nitrogen (N₂) inlet. And then, the copolymerization was carried out at 45 °C under N₂ atmosphere for 6 h. Finally, the AM/AA/NSFM copolymer was obtained after ethanol washing, drying, and pulverizing. The synthesis of AM/AA/NSFM is shown in Scheme 1 [20]. The AM/AA copolymer was synthesized by using the same method.

Scheme 1

Scheme 1: The synthesis of AM/AA/NSFM.

2.4. Characterization

Infrared (IR) spectra of AM/AA and AM/AA/NSFM were measured with KBr pellets using a Perkin Elmer RX-1 spectrophotometer. ¹H NMR spectrum of AM/AA/NSFM was recorded on a Bruker AC-E 200 spectrometer by dissolving the copolymer in D₂O and operating at 400 MHz. The elementary analysis of

AM/AA/NSFM was carried out with a Vario EL-III elemental analyzer. The microstructures of AM/AA and AM/AA/NSFM were observed by a scanning electron microscope (SEM). The weight-average molecular weight (M_w) of the copolymers was obtained by using a BI-200SM wide angle dynamic/static laser light scattering apparatus.

2.5. Rheological Property and Viscoelasticity

Rheological property and viscoelasticity measurements of the copolymers were conducted on a HAAKE RS 600 Rotational Rheometer (Germany). The shear rate was from 0.007 s^{-1} to 500 s^{-1} and the temperature was 65°C with a heating rate of $1.5^\circ\text{C}/\text{min}$, while the test system was binocular tube and the rotor was DG41Ti in rheological measurements. The scanning range of frequency (f) was 0.01-10 Hz, and the stress was 0.1 Pa by using the same test system and rotor in viscoelasticity measurements.

2.6. Mobility Control Ability

The mobility control ability of the copolymer solutions is characterized by the resistance factor (RF) and the residual resistance factor (RRF) [24-26]. The RF is calculated with the following equation:

$$RF = \left(\frac{K_w}{\mu_w} \right) / \left(\frac{K_p}{\mu_p} \right) \quad (1)$$

Where K_w is aqueous phase permeability, mD; K_p is polymer phase permeability, mD; μ_w is the viscosity of aqueous phase, mPa·s; μ_p is the viscosity of polymer phase, mPa·s.

The RRF is calculated with the following equation:

$$RRF = \frac{K_{wb}}{K_{wa}} \quad (2)$$

Where K_{wb} is aqueous phase permeability before polymer flooding, mD; K_{wa} is aqueous phase permeability after polymer flooding, mD.

2.7. Core Flooding Tests

Two Berea sandstone cores were used for core flooding experiments. The cores were dried at 65 °C, and then their length, diameter, porosity and gas permeability were measured by using a SCMS-B2 core multi-parameter measurement system. A Hassler core holder was used with 3.5 MPa confining pressure and 1.5 MPa backpressure. The core, after being saturated with brine, was saturated with crude oil (52.5 mPa·s at 65 °C) at 0.1-0.2 mL/min until the residual water saturation was obtained. After 72 h of aging, the core was flooded by the brine at 0.2 mL/min until water cut was up to 95%, and then the copolymer solution (0.2 wt%) was injected at 0.2 mL/min until water cut reach 95% once more [6, 26]. All the core flooding procedures were conducted at 65 °C. Chemical composition and total dissolved solids (TDS) of the brine are listed in Table 1. The maximum work pressure of the ISCO 260D syringe pump is 50 MPa, and its minimum and maximum displacement velocity are 0.001 and 50.000 mL/min, respectively. The EOR is calculated with the following equation:

$$EOR=E-E_w \quad (3)$$

Where EOR is enhanced oil recovery, %; E is the oil recovery of the whole displacement process, %; E_w is the oil recovery of water flooding, %.

Table 1: Composition and TDS of brine.

Table 1

Flow chart of the core flooding experiments is shown in Figure 1.

Figure 1

Figure 1: Flow chart of the core flooding experiments.

3. Results and Discussion

3.1. IR Spectra Analysis

The structures of AM/AA and AM/AA/NSFM were confirmed by IR spectra as illustrated in Figure 2. The

AM/AA/NSFM which was prepared using acrylic acid, acrylamide and NSFM by free radical polymerization was confirmed by strong absorptions at 3419 cm^{-1} (-NH stretching vibration and -OH stretching vibration), 2942 cm^{-1} (-CH₂ stretching vibration), 1675 cm^{-1} (C=O stretching vibration), 1402 cm^{-1} (C-N stretching vibration), 1100 cm^{-1} (Si-O-Si asymmetric stretching vibration), and 780 cm^{-1} (Si-O-Si symmetric stretching vibration) in the spectrum of AM/AA/NSFM [18, 20]. The peak at 3419 cm^{-1} was broad in the IR spectrum of AM/AA/NSFM partly due to the hydroxyl on nano-SiO₂ surface [20]. As expected, the IR spectra confirmed the presence of different monomers in AM/AA/NSFM.

Figure 2

Figure 2: IR spectra of AM/AA and AM/AA/NSFM.

3.2. ¹H NMR Analysis

The ¹H NMR spectrum of AM/AA/NSFM is shown in Figure 3. The chemical shift value at 1.29 ppm is due to the protons of [-CH₂-CH(Si(O-)₃)-]. The chemical shift value at 1.61 ppm is assigned to the protons of [-CH₂-CH(CONH₂)-] and [-CH₂-CH(COONa)-]. The protons of [-CH₂-CH(CONH₂)-] and [-CH₂-CH(COONa)-] appear at 2.17 ppm. And the characteristic peak due to the protons of [-CH₂-CH(Si(O-)₃)-] is observed at 2.38 ppm.

Figure 3

Figure 3: ¹H NMR spectrum of AM/AA/NSFM in D₂O.

3.3. Elementary Analysis of AM/AA/NSFM

The elementary analysis of the AM/AA/NSFM copolymer was carried out using a Vario EL-III elemental analyzer. The content of different element in the copolymer can be obtained by detecting the gases, which are the decomposition products of the copolymer at high temperature. Theoretical value: 0.21% (Si %), 45.4% (C %), 5.4% (H %); Found value: 0.17% (Si %), 40.1% (C %), 4.8% (H %).

3.4. Microscopic Structure

The microscopic structures of AM/AA and AM/AA/NSFM were observed through SEM at room temperature. The copolymers solution samples (0.05 wt%) were prepared with distilled water and cooled with liquid nitrogen, and then these samples were evacuated in order to keep original appearance of the copolymers as far as possible. As shown in Figure 4 and 5, the molecular chains of copolymer were obviously changed when NSFM was introduced into the AM/AA copolymer. Compared with the images of AM/AA, the molecular coils of AM/AA/NSFM were composed of many micro-nano structure units, and the force between these units could be heightened due to Si-O and C-Si bond. In addition, this structure may increase retention of AM/AA/NSFM on the rock face which is favorable to mobility control and EOR.

Figure 4

Figure 4: SEM images of AM/AA.

Figure 5

Figure 5: SEM images of AM/AA/NSFM.

3.5. Weight-Average Molecular Weight

Five different concentrations (10, 20, 40, 60, 80 mg/L) copolymer solutions were prepared with distilled water and filtered using a 0.5 µm Millipore Millex-LCR filter before static laser light scattering (SLLS) experiments. The M_w of AM/AA and AM/AA/NSFM can be calculated with the following equation [27]:

$$\frac{KC}{R_{vv}(q)} \cong \frac{I}{M_w} \left(1 + \frac{1}{3} \langle R_g^2 \rangle q^2\right) \quad (4)$$

Where K is a constant; C is the concentration of copolymer solution, g/mL; $R_{vv}(q)$ is the Rayleigh ratio; $\langle R_g^2 \rangle$ is the average radius of gyration, nm; and $q = (4\pi/\lambda) \sin(\theta/2)$ with λ , θ , and n being the scattering angle, the wavelength of light in vacuo, and the solvent refractive index, respectively.

The M_w of AM/AA and AM/AA/NSFM is 1.33×10^7 g/mol and 1.32×10^7 g/mol, respectively (for the details, see supporting information).

3.6. Shear Resistance

The viscosity vs. shear rate curves of AM/AA and AM/AA/NSFM (0.2 wt%) are shown in Figure 6(a). It was clearly found that AM/AA and AM/AA/NSFM revealed non-Newtonian shear-thinning behavior. Hence, with the increase of the shear rate (from 0.007 to 500 s⁻¹), the viscosity of copolymer solutions dropped obviously. The results indicated that AM/AA/NSFM had better viscosifying property than AM/AA, and the viscosity of AM/AA/NSFM was higher than that of AM/AA at 500 s⁻¹ shear rate (18.6 mPa·s vs. 8.7 mPa·s). Furthermore, AM/AA and AM/AA/NSFM were investigated by changing the shear rate from 124 s⁻¹ to 500 s⁻¹ and from 500 s⁻¹ to 124 s⁻¹ around (Figure 6(b) and (c)). Compared with AM/AA, AM/AA/NSFM had higher retention rate of viscosity (85% vs. 68%) when one cycle was completed. This phenomenon may support the Si-O and C-Si bond in AM/AA/NSFM can improve the shear tolerance of the copolymer. And the structures of AM/AA/NSFM may be restored after being sheared.

(a)

(b)

(c)

Figure 6

Figure 6: (a) Effect of shear rate on viscosity; (b) Shear resistance of AM/AA; (c) Shear resistance of AM/AA/NSFM. The copolymers solutions (0.2 wt%) were prepared with distilled water.

3.7. Viscoelasticity Measurements

The viscoelasticity curves of AM/AA and AM/AA/NSFM solutions (0.2 wt%) are shown in Figure 7. When the frequency was lower than 1 Hz, the viscous modulus (G'') of AM/AA/NSFM was higher than the elastic modulus (G'); when the frequency was higher than 1 Hz, the situation was just the opposite. However, the G'' of AM/AA was higher than G' in the entire frequency scan range. Compared with

AM/AA, AM/AA/NSFM exhibited higher G' and G'' under the same conditions. This phenomenon may support the micro-nano structure units in AM/AA/NSFM can enhance the acting force of polymer molecular coils.

Figure 7

Figure 7: Viscoelasticity of AM/AA and AM/AA/NSFM at 65 °C. The copolymers solutions (0.2 wt%) were prepared with distilled water.

3.8. Temperature Tolerance

AM/AA and AM/AA/NSFM solutions were prepared with distilled water. And the viscosity of copolymer solutions was measured by the Brookfield DV-3 viscometer at different temperatures. The viscosity vs. temperature curves of AM/AA and AM/AA/NSFM solutions are shown in Figure 8. The test results showed that the AM/AA/NSFM solution had higher viscosity at the same temperature. Additionally, the viscosity of AM/AA/NSFM solution decreased less than that of AM/AA when temperature was above 80 °C. This may support the stable Si-O and C-Si bond can obviously improve temperature tolerance of AM/AA/NSFM.

Figure 8

Figure 8: Viscosity vs. temperature for AM/AA and AM/AA/NSFM solution. The viscosity of copolymer solution (0.5 wt%) were measured by Brookfield DV-3 viscometer at 7.34 s^{-1} using 62# rotor (rotation speed: 18.8 r/min).

3.9. Salt Tolerance

As shown in Figure 9(a, b, c), with the increase of salt concentration (NaCl, CaCl₂, MgCl₂·6H₂O), the viscosity of copolymers decrease rapidly, and then it kept at a low value. It was found that AM/AA and AM/AA/NSFM had less satisfactory salt tolerance to Na⁺ or Ca²⁺ than Mg²⁺ under the same conditions. Compared with AM/AA, AM/AA/NSFM exhibited no obvious advantage in salt tolerance due to the

shrinking of copolymer chain with the increase of salt concentration.

(a)

(b)

(c)

Figure 9

Figure 9: Salt tolerance ((a) NaCl, (b) CaCl₂, (c) MgCl₂·6H₂O) of AM/AA and AM/AA/NSFM solutions (0.5 wt%) at 20 °C.

The viscosity of copolymer solution were measured by Brookfield DV-3 viscometer at 7.34 s⁻¹ using 62# rotor (rotation speed: 18.8 r/min) or 61# rotor (rotation speed: 18.5 r/min).

3.10. Mobility Control Ability

The core barrel was packed with quartz sand which was washed by hydrochloric acid and distilled water for several times. The injection rate of brine (sodium chloride concentration was 0.5 wt%) and polymer solution prepared with the brine was 2.0 mL/min with the ISCO 260D syringe pump. Experiments were carried out at 65 °C in an incubator with precision of 0.1 °C. And the injection pressure was collected by a pressure sensor with precision of 0.0001 MPa. The flow characteristic curves of AM/AA and AM/AA/NSFM in porous media are shown in Figure 10.

Figure 10

Figure 10: Flow characteristic curves of AM/AA and AM/AA/NSFM solution (0.2 wt%). The length and internal diameter of the core barrel were 25 cm and 2.5 cm, respectively.

As shown in Figure 10, the AM/AA/NSFM solution could establish much higher RF and RRF than that of the AM/AA solution under the same conditions (RF: 16.52 vs. 12.17, RRF: 3.63 vs. 2.59). This is to say the AM/AA/NSFM solution has stronger mobility control ability which is favorable to enhance oil recovery due to the higher viscosity retention rate and microstructure. In addition, it was found that AM/AA/NSFM

revealed higher retention than AM/AA (83 mg vs. 55 mg) by material balance calculations (for the details, see supporting information). This may support that the huge surface area of micro-nano structure units of AM/AA/NSFM can enhance the adsorption which may play an important role in improving mobility control.

3.11. Enhanced Oil Recovery

As shown in Table 2, the EOR of AM/AA/NSFM solution (0.2 wt%) was 20.10% compared with water flooding at 65 °C. However, the EOR of AM/AA solution (0.2 wt%) was 14.22% under the same conditions. The EOR results showed that AM/AA/NSFM revealed more superior ability of oil displacement. As shown in Figure 11, compared with AM/AA, AM/AA/NSFM exhibited stronger ability of reducing water cut and establishing flow resistance in polymer flooding process. This phenomenon may support the sweep efficiency is obviously improved by AM/AA/NSFM due to the excellent mobility control capability in porous media.

Table 2: The relevant core properties and the results of core flooding experiments.

Table 2

Figure 11

Figure 11: Core flooding experiments results of AM/AA/NSFM and AM/AA (0.2 wt%) at 65 °C..

4. Conclusions

A novel copolymer containing nano-SiO₂ was synthesized by free radical polymerization using AM, AA, and NSFM as raw materials. The AM/AA/NSFM copolymer was characterized by IR spectrum, ¹H NMR spectrum, elemental analysis, and scanning electron microscope. The solution properties, such as rheological property, viscoelasticity, temperature tolerance, salt tolerance, mobility control ability, and oil displacement efficiency of the copolymer, were investigated under different conditions. The results indicated that the

copolymer containing nano-SiO₂ possessed moderate or good shear resistance, temperature tolerance, and mobility control ability as EOR chemical.

Conflict of Interests

The author declares no possible conflict of interests.

Acknowledgments

This work was supported by the Open Fund (PLN1212) of State Key Laboratory of Oil and Gas Reservoir Geology and Exploitation (Southwest Petroleum University) and the Specialized Research Fund for the Doctoral Program of Higher Education (20125121120011).

References

1. N. Mungan, F.W. Smith, J.L. Thompson, O. Sinclair, and C. Gas, "Some aspects of polymer floods," *Journal of Petroleum Technology*, vol. 18, no. 9, pp. 1143-1150, 1966.
2. B.S. Shiran and A. Skauge, "Enhanced oil recovery (EOR) by combined low salinity water/polymer flooding," *Energy Fuels*, vol. 27, no. 3, pp. 1223-1235, 2013.
3. C.R. Zhong, R.H. Huang, X. Zhang, and H. Dai, "Synthesis, characterization, and solution properties of an acrylamide-based terpolymer with butyl styrene," *Journal of Applied Polymer Science*, vol. 103, no. 11, pp. 4027-4038, 2007.
4. T. Rho, J. Park, C. Kim, H. Yoon, and H. Suh, "Degradation of polyacrylamide in dilute solution," *Polymer Degradation and Stability*, vol. 51, no. 3, pp. 287-293, 1996.
5. D.A.Z. Wever, F. Picchioni, and A.A. Broekhuis, "Polymers for enhanced oil recovery: a paradigm for structure-property relationship in aqueous solution," *Progress in Polymer Science*, vol. 36, no. 11, pp. 1558-1628, 2011.
6. Z.B. Ye, G.J. Gou, S.H. Gou, W.C. Jiang, and T.Y. Liu, "Synthesis and characterization of a water-soluble sulfonates copolymer of acrylamide and N-Allylbenzamide as enhanced oil recovery chemical," *Journal of Applied Polymer Science*, vol. 128, no. 3, pp. 2003-2011, 2013.
7. S.H. Chang and I.J. Chung, "Effect of shear flow on polymer desorption and latex dispersion stability in the presence of adsorbed polymer," *Macromolecules*, vol. 24, no. 2, pp. 567-571, 1991.

8. L. Xue, U.S. Agarwal, and P.J. Lemstra, "Shear degradation resistance of star polymers during elongational flow," *Macromolecules*, vol. 38, no. 21, pp. 8825–8832, 2005.
9. J. Zheng, P. Cui, X.Y. Tian, and K. Zheng, "Pyrolysis studies of polyethylene terephthalate/silica nanocomposites," *Journal of Applied Polymer Science*, vol. 104, no. 1, pp. 9–14, 2007.
10. L.I. Rueda, L.G. Hernandez, and C.C. Anton, "Effect of the textural characteristics of the new silicas on the dynamic properties of Styrene-Butadiene Rubber (SBR) vulcanizates," *Polymer Composites*, vol. 9, no. 3, pp. 204–208, 1988.
11. H.S. Xia and Q. Wang, "Preparation of conductive polyaniline/nanosilica particle composites through ultrasonic irradiation," *Journal of Applied Polymer Science*, vol. 87, no. 11, pp. 1811–1817, 2003.
12. X. Wang, X.H. Zhao, M.Z. Wang, and Z.G. Shen, "The effects of atomic oxygen on polyimide resin matrix composite containing nano-silicon dioxide," *Nuclear Instruments and Methods in Physics Research Section B: Beam Interactions with Materials and Atoms*, vol. 243, no. 2, pp. 320–324, 2006.
13. Y. Li, J. Yu, and Z.X. Guo, "The influence of interphase on nylon-6/nano-SiO₂ composite materials obtained from in situ polymerization," *Polymer International*, vol. 52, no. 6, pp. 981–986, 2003.
14. V. A. Bershtein, L. M. Egorova, P. N. Yakushev, P. Pissis, P. Sysel, and L. Brozova, "Molecular dynamics in nanostructured polyimide–silica hybrid materials and their thermal stability," *Journal of Polymer Science Part B: Polymer Physics*, vol. 40, no. 10, pp. 1056–1069, 2002.
15. N. D. Alberola, K. Benzarti, C. Bas, and Y. Bomal, "Interface effects in elastomers reinforced by modified precipitated silica," *Polymer Composites*, vol. 22, no. 2, pp. 312–325, 2001.
16. A. Voronov, A. Kohut, A. Synytska, and W. Peukert, "Mechanochemical modification of silica with poly(1-vinyl-2-pyrrolidone) by grinding in a stirred media mill," *Journal of Applied Polymer Science*, vol. 104, no. 6, pp. 3708–3714, 2007.
17. H. Zou, S.S. Wu, and J. Shen, "Polymer/silica nanocomposites: preparation, characterization, properties, and applications," *Chemical Reviews*, vol. 108, no. 9, pp. 3893–3957, 2008.
18. G.H. Hsiue, W.J. Kuo, Y.P. Huang, and R.J. Jeng, "Microstructural and morphological characteristics of PS–SiO₂ nanocomposites," *Polymer*, vol. 41, no. 8, pp. 2813–2825, 2000.
19. W. Wang, B.H. Gu, "Self-assembly of two- and three-dimensional particle arrays by manipulating the hydrophobicity of silica nanospheres," *The Journal of Physical Chemistry B*, vol. 109, no. 47, pp. 22175–22180, 2005.

20. B.J. Kim and K.S. Kang, "Fabrication of a crack-free large area photonic crystal with colloidal silica spheres modified with vinyltriethoxysilane," *Crystal Growth & Design*, vol. 12, no. 8, pp. 4039–4042, 2012.
21. A.V. Biradar, A.A. Biradar, and T. Asefa, "Silica-dendrimer core-shell microspheres with encapsulated ultrasmall palladium nanoparticles: efficient and easily recyclable heterogeneous nanocatalysts," *Langmuir*, vol. 27, no. 23, pp. 14408–14418, 2011.
22. Z. Meng, C.Y. Xue, Q.H. Zhang, X.H. Yu, K. Xi, and X.D. Jia, "Preparation of highly monodisperse hybrid silica nanospheres using a one-step emulsion reaction in aqueous solution," *Langmuir*, vol. 25, no. 14, pp. 7879–7883, 2009.
23. Z. Wu, H. Han, W. Han, B. Kim, K.H. Ahn, and K. Lee, "Controlling the hydrophobicity of submicrometer silica spheres via surface modification for nanocomposite applications," *Langmuir*, vol. 23, no. 14, pp. 7799–7803, 2007.
24. R. Ponnampati, O. Karazincir, E. Dao, R. Ng, K.K. Mohanty, and R. Krishnamoorti, "Polymer-functionalized nanoparticles for improving waterflood sweep efficiency: characterization and transport properties," *Industrial & Engineering Chemistry Research*, vol. 50, no. 23, pp. 13030–13036, 2011.
25. C.R. Zhong, L. Ye, H. Dai, and R.H. Huang, "Flourescent probe and ESEM morphologies of a acrylamide-based terpolymer in aqueous solution," *Journal of Applied Polymer Science*, vol. 103, no. 1, pp. 277–286, 2007.
26. L.T. Shi, Z.B. Ye, Z. Zhang, C.J. Zhou, S.S. Zhu, and Z.D. Guo, "Necessity and feasibility of improving the residual resistance factor of polymer flooding in heavy oil reservoirs," *Petroleum Science*, vol. 7, no. 2, pp. 251–256, 2010.
27. X.H. Wang, X.P. Qiu, and C. Wu, "Comparison of the coil-to-globule and the globule-to-coil transitions of a single Poly(N-isopropylacrylamide) homopolymer chain in water," *Macromolecules*, vol. 31, no. 9, pp. 2972–2976, 1998.

Table 1: Composition and TDS of brine.

Composition	NaCl	KCl	CaCl ₂	MgCl ₂ ·6H ₂ O	Na ₂ SO ₄	NaHCO ₃	TDS
Content (g/L)	8.495	0.149	0.764	2.154	0.125	0.428	10.951

Table 2: The relevant core properties and the results of core flooding experiments.

Copolymer	Cores	Length (cm)	Diameter (cm)	Porosity (%)	Permeability (mD)	Swi (%)	E (%)	Ew (%)	EOR (%)
AM/AA	1#	8.84	3.77	23.11	937.03	19.18	45.73	31.51	14.22
AM/AA/NSFM	2#	8.92	3.78	23.05	926.28	19.37	52.85	31.75	20.10

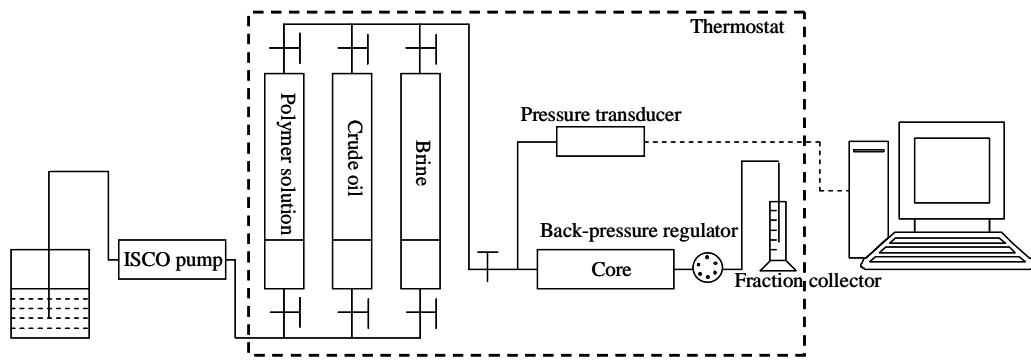


Figure 1: Flow chart of the core flooding experiments.

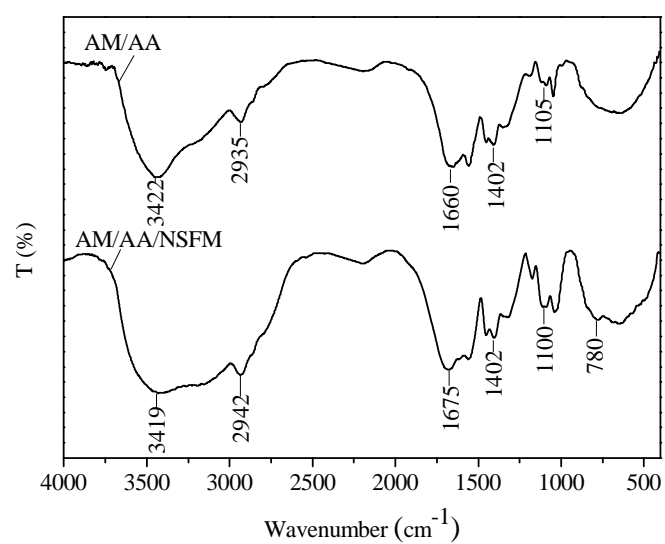


Figure 2: IR spectra of AM/AA and AM/AA/NSFM.

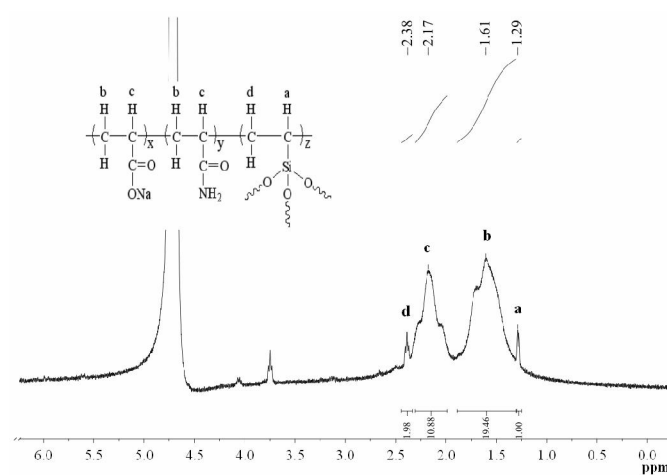


Figure 3: ^1H NMR spectrum of AM/AA/NSFM in D_2O .

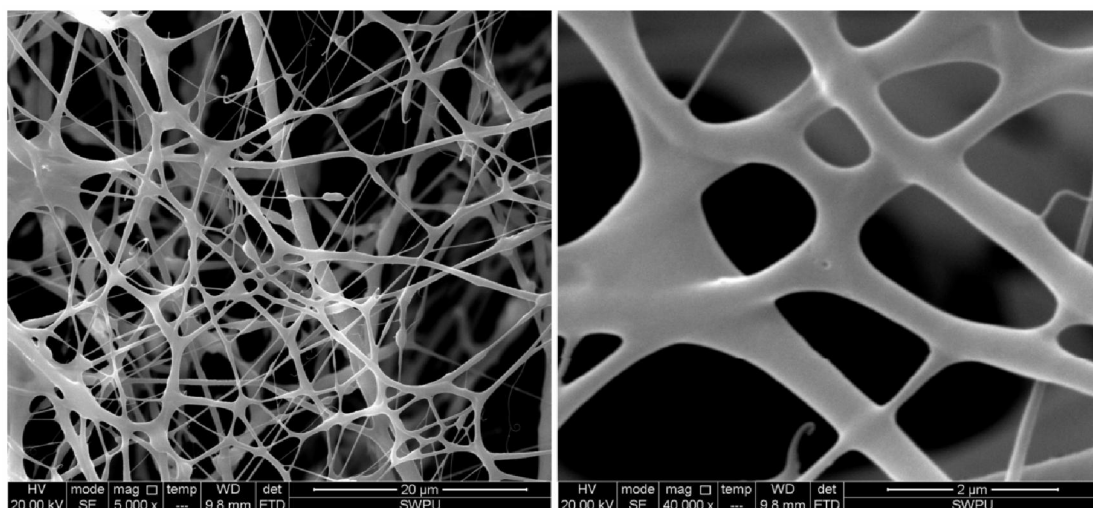


Figure 4: SEM images of AM/AA.

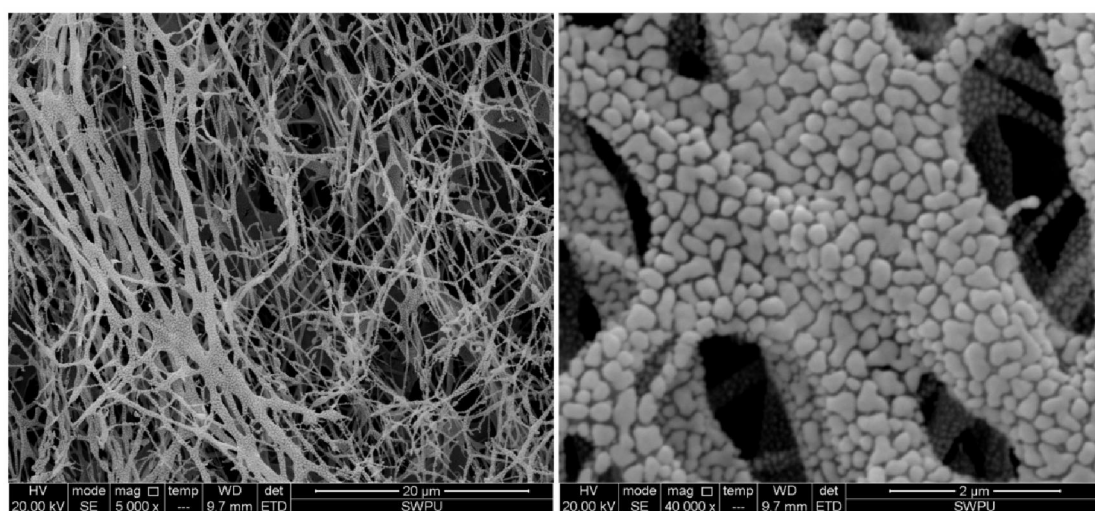
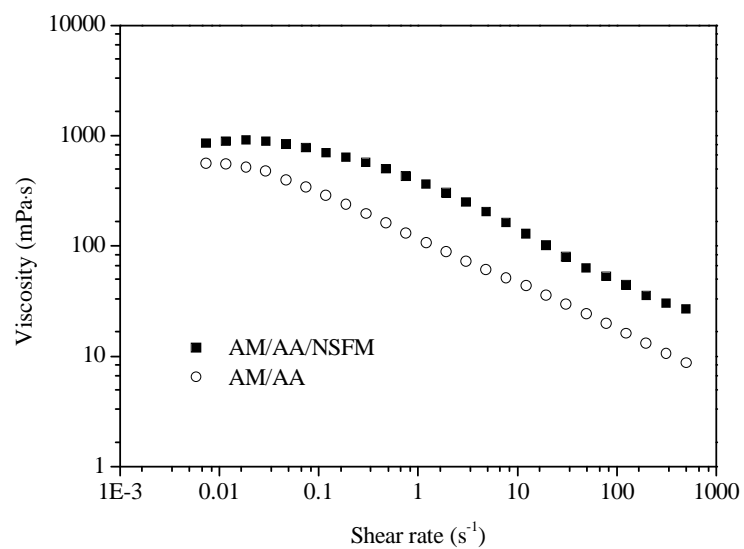
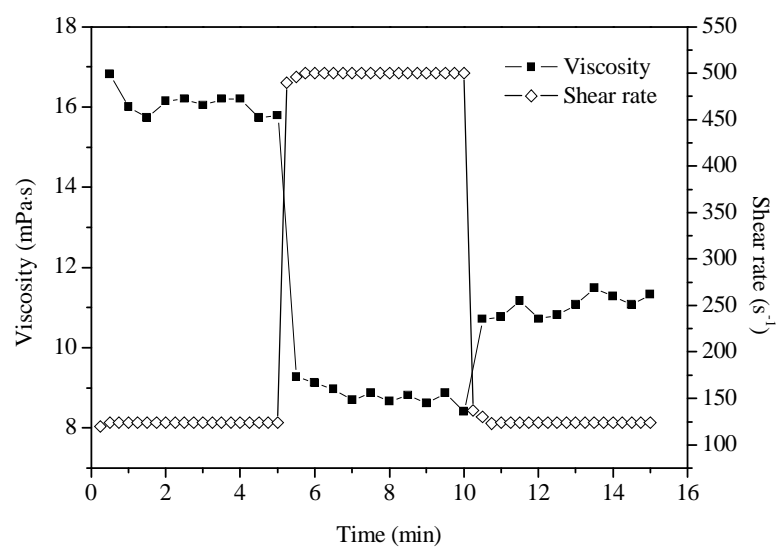


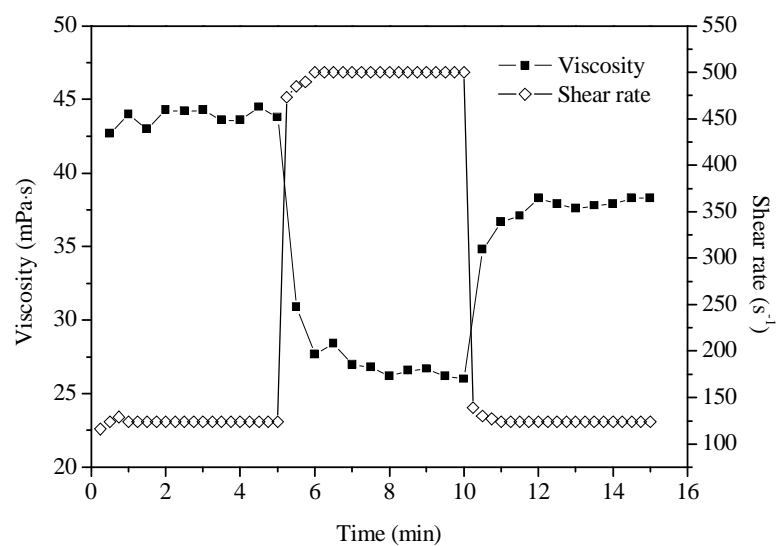
Figure 5: SEM images of AM/AA/NSFM.



(c)



(b)



(c)

Figure 6: (a) Effect of shear rate on viscosity; (b) Shear resistance of AM/AA; (c) Shear resistance of AM/AA/NSFM. The copolymers solutions (0.2 wt%) were prepared with distilled water.

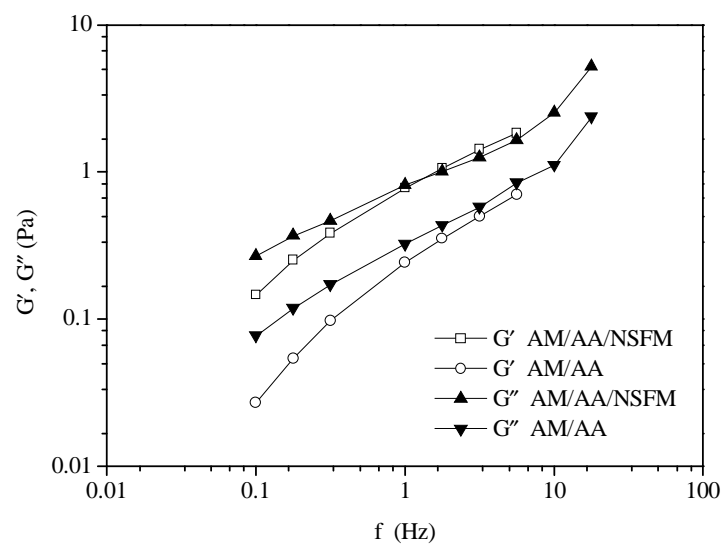


Figure 7: Viscoelasticity of AM/AA and AM/AA/NSFM at 65 °C. The copolymers solutions (0.2 wt%) were prepared with distilled water.

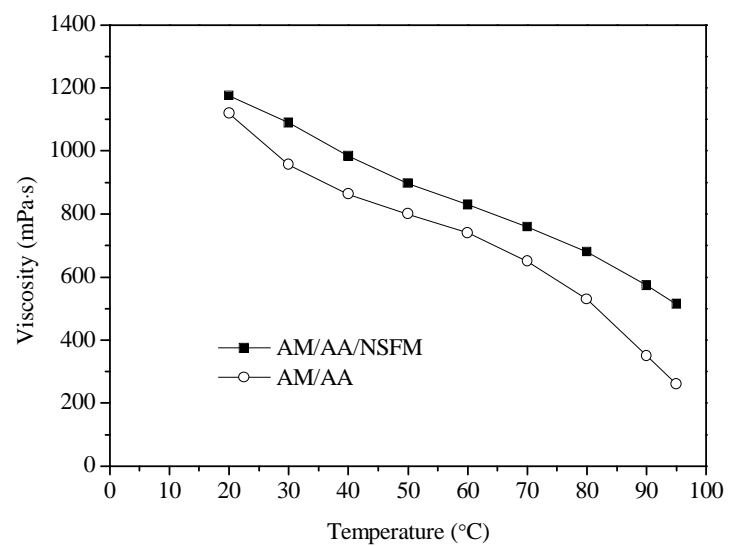
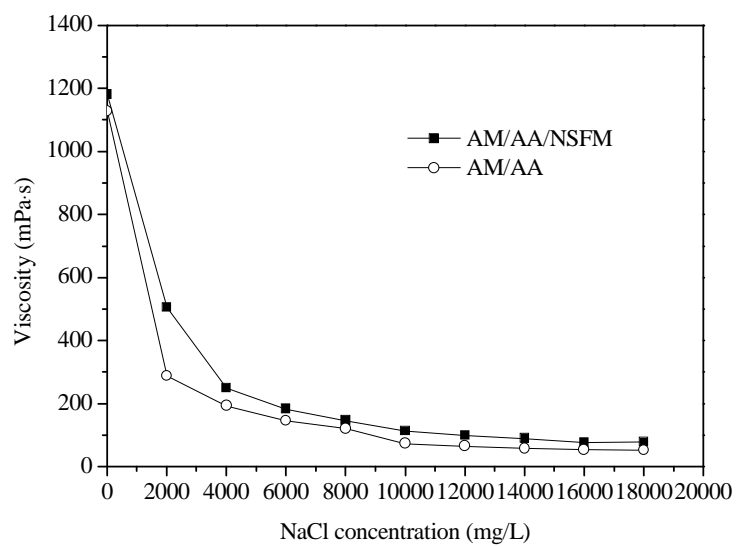
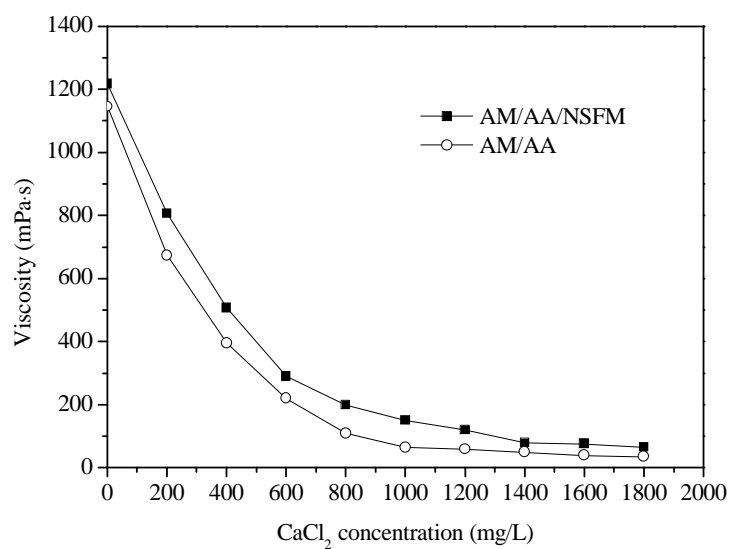


Figure 8: Viscosity vs. temperature of AM/AA and AM/AA/NSFM solution. The viscosity of copolymer solution (0.5 wt%)

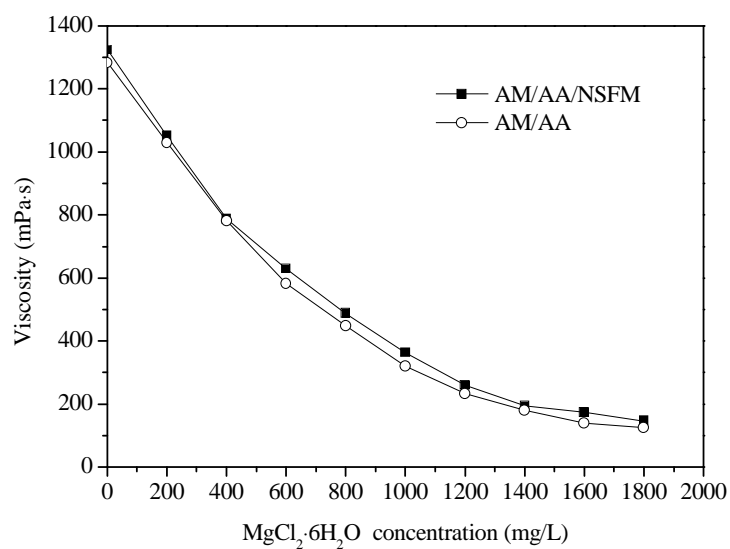
were measured by Brookfield DV-3 viscometer at 7.34 s^{-1} using 62# rotor (rotation speed: 18.8 r/min).



(a)



(b)



(c)

Figure 9: Salt tolerance ((a) NaCl, (b) CaCl₂, (c) MgCl₂·6H₂O) of AM/AA and AM/AA/NSFM solutions (0.5 wt%) at 20 °C.

The viscosity of copolymer solution were measured by Brookfield DV-3 viscometer at 7.34 s⁻¹ using 62# rotor (rotation speed: 18.8 r/min) or 61# rotor (rotation speed: 18.5 r/min).

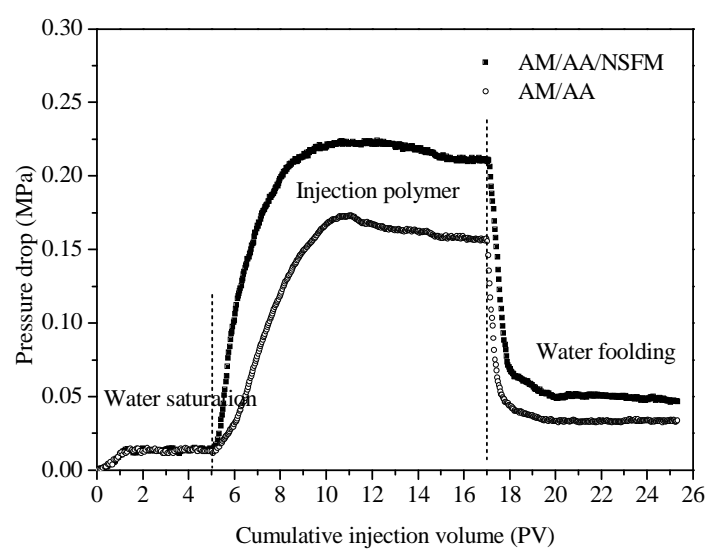


Figure 10: Flow characteristic curves of AM/AA and AM/AA/NSFM solution (0.2 wt%). The length and internal diameter of the core barrel were 25 cm and 2.5 cm, respectively.

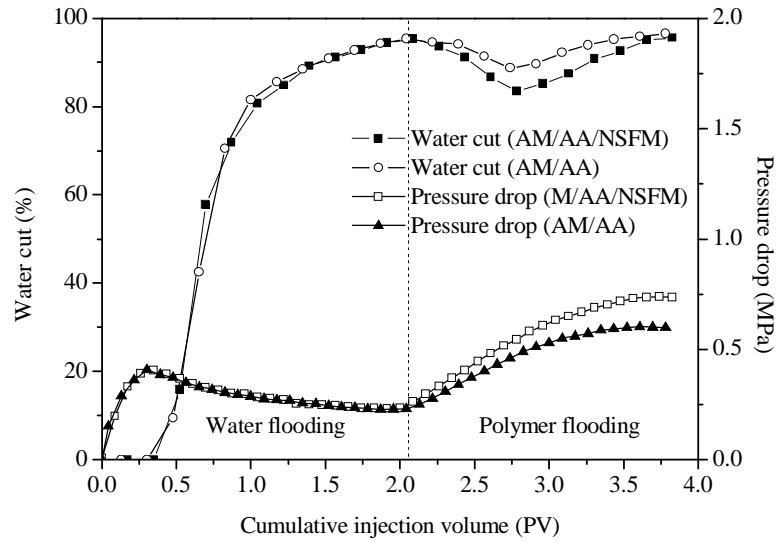
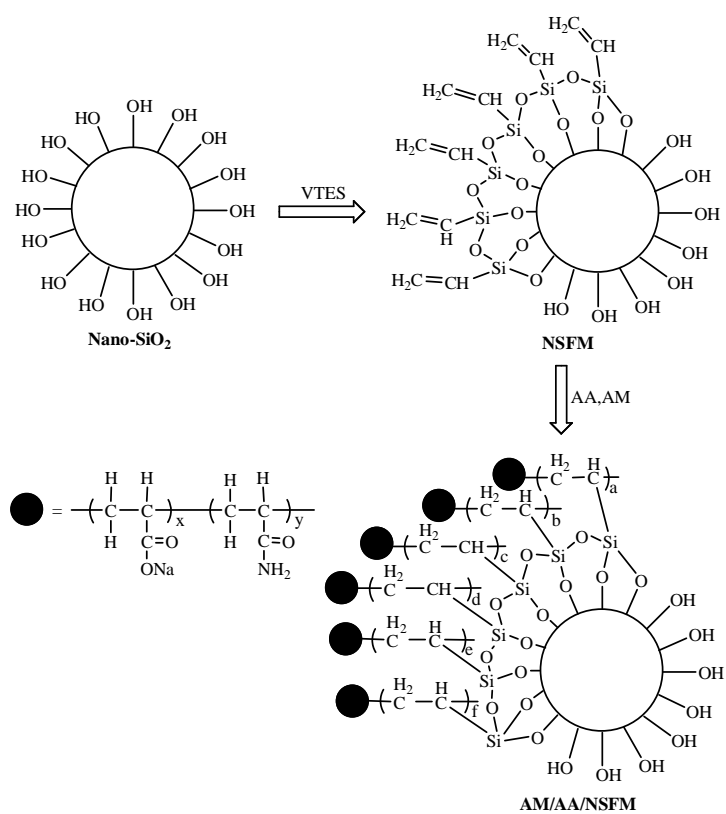


Figure 11: Core flooding experiments results of AM/AA/NSFM and AM/AA (0.2 wt%) at 65 °C.



Scheme 1: The synthesis of AM/AA/NSFM.